A High-Precision Positioning Method Without Ground Control Points for Mosaic Aerial Survey Camera

Chang Yu [1], Xiu Liu [2], Yansong Duan [1]

[1] School of Remote Sensing and Information Engineering, Wuhan University, Wuhan 430079, China - (yuchang_, ysduan)@whu.edu.cn
[2] Beijing Institute of Space Mechanics&Electricity,Beijing 100094, China - (liuxiu0725@163.com)

Keywords: Mosaic aerial camera; GCP-free; Cloud control; Collimation axis calibration; Bundle adjustment.

Abstract

Mosaic aerial survey cameras facilitate large-format imaging by integrating multiple lenses and sensors. Nevertheless, the inherent complexity of their structural design gives rise to collimation axis eccentricity errors between the Position and Orientation System (POS) and the camera's optical center. Conventional methods, which rely on Ground Control Points (GCPs), fall short of fulfilling the demands for high-precision and high-efficiency surveying and mapping tasks. This manuscript presents a ground-control-point-free positioning approach grounded in "cloud control" photogrammetry technology. Leveraging publicly available Google images and Shuttle Radar Topography Mission (SRTM) elevation data as reference sources, a simultaneous solution for the exterior orientation elements of images and the collimation axis eccentricity angle of the Inertial Measurement Unit (IMU) is achieved through bundle adjustment. This process enables rigorous geometric calibration of the camera system. Experimental findings demonstrate that, in the absence of ground control points, the proposed method attains a planar positioning accuracy of 0.29 meters in the x-direction and 0.40 meters in the y-direction, along with a vertical positioning accuracy of 0.78 meters. These results satisfy the surveying and mapping accuracy criteria for a 1:500 scale, underscoring its significant potential for practical engineering applications.

1. Introduction

The rapid advancement of aerospace remote sensing technology has established aerial surveying and mapping as a critical tool in domains such as national land surveys, urban planning, and emergency response. Conventional single-camera aerial survey systems, however, face inherent limitations due to their restricted field of view and base-to-height ratio, making it challenging to simultaneously achieve high-efficiency, large-area image acquisition and high-precision geometric positioning (Zuxun ZHANG et al. 2025). To address these constraints, multi-lens mosaic aerial camera systems have been developed. These systems integrate multiple lens-CMOS (Complementary Metal Oxide Semiconductor) sensor units with a Position and Orientation System (POS), enabling synergistic operation for efficient aerial photography and precise geometric positioning. Compared to traditional single-lens CCD cameras, multi-lens mosaic cameras offer distinct advantages, including lower noise, a wider dynamic range, and the capability to capture ultra-large-format imagery. Despite these benefits, the complex architecture of these cameras—comprising multiple independent lenses, each with a focal plane often consisting of multiple CMOS sub-arrays—introduces significant challenges for high-precision surveying and mapping applications.

The onboard POS, which typically integrates a Global Navigation Satellite System (GNSS) receiver and an Inertial Measurement Unit (IMU), provides real-time measurements of the carrier's spatial position (X,Y,Z) and attitude (φ,ω,κ) in a defined coordinate system. The accuracy of this direct georeferencing is contingent upon the precise alignment between the POS measurement center and the camera's perspective center (Salas López et al. 2022). In a mosaic camera configuration, this requirement is complicated by the spatial distribution of multiple lenses and inevitable deviations introduced during mechanical assembly. Consequently, the POS cannot physically coincide with the optical center of each sub-camera (Mikš and Novák 2018). This non-concentric characteristic introduces collimation axis errors, which significantly degrade the final geolocation accuracy. Therefore, the precise calibration of the geometric relationship between the camera system and the POS, specifically the correction of boresight angles offsets, is paramount for enhancing the positioning performance of mosaic cameras.

In traditional photogrammetry, collimation axis errors can be calibrated using Ground Control Points (GCPs). However, this approach presents two major drawbacks: Firstly, the field deployment and measurement of GCPs are time-consuming, often rendering them impractical for emergency mapping missions with stringent timeliness requirements. Secondly, even when GCPs can be established, their spatial representativeness and measurement accuracy can be substantially compromised in complex terrains (e.g., undulating landscapes, vegetated areas, or dense urban environments), leading to systematic biases in the calibration results. Hence, there is a pressing need to develop high-precision positioning methodologies that operate independently of ground control to bolster the application capabilities of mosaic cameras in specialized scenarios such as emergency response.

To address these limitations, extensive research has been conducted in the field of POS-assisted aerial photogrammetry. Jacobsen (Jacobsen 2002) pioneered the application of POS systems in aerial photogrammetry, enabling the direct acquisition of the six exterior orientation parameters for aerial images. Lu et al. (Heng Lu et al. 2011) enhanced the POS data processing algorithm, thereby improving the direct georeferencing accuracy of UAV imagery. Xu et al. (Qiuhui Xu 2013) facilitated integrated processing by establishing a mapping relationship between distorted and undistorted images, enabling simultaneous image distortion correction and POS data calibration. Ma and Wang (Huaiwu Ma and Junqiang Wang 2014) incorporated Real-Time Kinematic (RTK) carrier-phase

differential GNSS technology with POS data to enhance image positioning accuracy.J Liu et al. (Liu et al. 2024) proposed a geolocation method that integrated POS-derived parameters with aerial triangulation, using the raw POS data as initial values in a bundle adjustment to solve for refined exterior orientation parameters and ground coordinates.

Regarding the calibration of boresight errors, various theoretical and methodological frameworks have been proposed to improve the geometric consistency between the POS and the camera. Yuan et al. (Xiuxiao Yuan et al. 2006) introduced a calibration method based on the analysis of discrepancies between the POS-measured attitude angles and the photogrammetrically derived exterior orientation angles, establishing a foundation for systematic error compensation. Fu and Zhao (Jianhong Fu and Shuangming Zhao 2011) developed a mathematical model linking the image nadir point to boresight error based on vanishing point theory, achieving calibration without the need for a physical calibration field or GCPs, which provided a practical solution for urban aerial photography. Jia et al. (Xin Jia et al. 2019) further advanced POS calibration theory for mosaic imaging systems by revealing the opposing characteristics of exterior orientation linear element errors between odd and even flight strips.

In the domain of GCP-free positioning, research focus has progressively shifted from reliance on GCPs towards multi-source data fusion and virtual control point technologies. Gong et al. (Adu Gong et al. 2010) proposed a method for geometric correction and mosaicking of UAV images without GCPs, promoting the adoption of uncontrolled processing in UAV applications. Cheng et al. (Hao Cheng et al. 2016) presented a dual-image stereo positioning method for UAVs that utilized continuously captured overlapping images and POS data to directly resolve 3D coordinates of targets, achieving a horizontal accuracy better than 15 meters in areas lacking reference data or with indistinct features. Sun et al. (Yushan Sun et al. 2018) constructed “average” virtual control points and combined them with a rational function model (RFM) adjustment, achieving a positioning accuracy better than 6 meters for ZY-3 satellite imagery without GCPs. Ding (Shulei Ding 2024) proposed a multi-modal fusion positioning method leveraging public DEMs (Digital Elevation Model) and LiDAR (Light Detection and Ranging) point clouds. Virtual control points were extracted via Self-Organizing Feature Map (SOFM) matching, and high-precision positioning was realized through RFM-based block adjustment, demonstrating significant advantages in complex terrains and overseas areas. More recently, Zhu et al. (Zhu et al. 2025) introduced a “cloud control” method, where airborne LiDAR point clouds were used to generate a network of virtual control points, successfully enabling high-precision aerial triangulation and 3D modeling without GCPs in a hybrid block comprising both historical and contemporary aerial imagery.

2. Methods

2.1 Technical Workflow

The proposed workflow for geopositioning without GCPs, illustrated in Figure 1, comprises four sequential steps: (1) Initial rough orthorectification and comprehensive preprocessing of raw aerial images using onboard POS data to establish a preliminary geometric correction framework; (2) Extraction of virtual control points from historical imagery through an innovative “cloud control” strategy, leveraging existing geospatial data to establish reliable reference points and eliminate the need for field-based GCP collection; (3) Implementation of a rigorous bundle adjustment to simultaneously refine the exterior orientation parameters of the imaging system and the collimation axis angle of the IMU, ensuring accurate recovery of the camera's spatial position and attitude during image acquisition; (4) Generation of high-quality orthophotos based on the corrected POS data derived from the adjustment, followed by a comprehensive accuracy assessment to validate geolocation precision and ensure the reliability of the final mapping products.

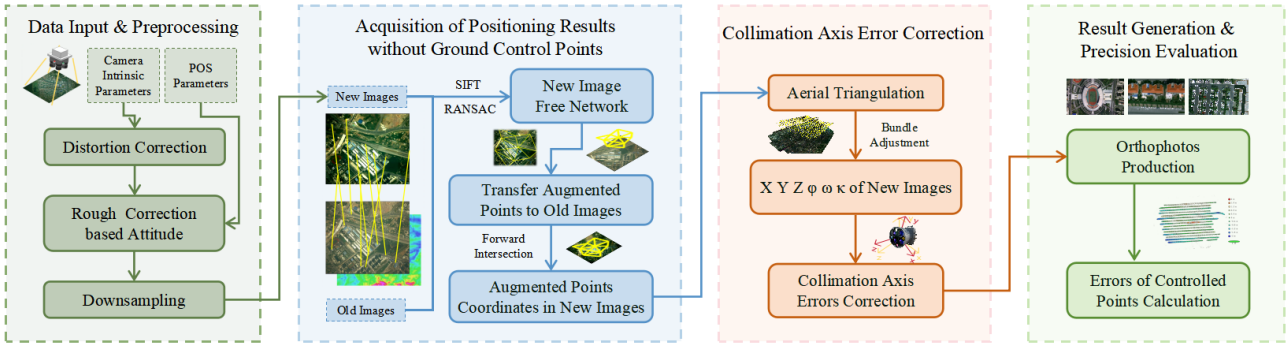

Figure 1.Technical workflow for positioning of mosaic aerial survey camera without ground control points.

2.2 Collimation Axis Calibration Method

The mosaic aerial survey camera is a large-format camera using CMOS sensor technology, composed of four panchromatic and four multispectral cameras. Under ideal conditions, the image point (x,y) and the object point (X,Y,Z) satisfy the collinear condition equation (formula (1)):

$$\begin{cases} x-x_0 = -f\dfrac{a_1(X-X_S)+b_1(Y-Y_S)+c_1(Z-Z_S)}{a_3(X-X_S)+b_3(Y-Y_S)+c_3(Z-Z_S)} \\ y-y_0 = -f\dfrac{a_2(X-X_S)+b_2(Y-Y_S)+c_2(Z-Z_S)}{a_3(X-X_S)+b_3(Y-Y_S)+c_3(Z-Z_S)} \end{cases} \quad (1)$$

To eliminate the collimation axis eccentricity error of the mosaic aerial survey camera, a systematic error correction term is introduced into the image point coordinates. The enhanced imaging model, formulated as a self-calibration model, is expressed in formula (2):

$$\begin{cases} x\text{-}x_0 = -f\dfrac{a_1(X\text{-}X_S)+b_1(Y\text{-}Y_S)+c_1(Z\text{-}Z_S)}{a_3(X\text{-}X_S)+b_3(Y\text{-}Y_S)+c_3(Z\text{-}Z_S)}+\Delta x \\ y\text{-}y_0 = -f\dfrac{a_2(X\text{-}X_S)+b_2(Y\text{-}Y_S)+c_2(Z\text{-}Z_S)}{a_3(X\text{-}X_S)+b_3(Y\text{-}Y_S)+c_3(Z\text{-}Z_S)}+\Delta y \end{cases} \quad (2)$$

Where, (x_0,y_0,f) is the interior orientation element, (X_S,Y_S,Z_S) is the exterior orientation line element, and a_i,b_i,c_i is the direction cosine matrix element.

Considering the collimation axis eccentricity angle of IMU and the drift errors of GNSS and IMU, the error equation of POS assisted integrated sensor system bundle adjustment is derived as formula (3):

$$\begin{cases} V_1 = A_1X_1 + A_2X_2 + A_3X_3 - L_1 & P_1 \\ V_2 = B_1X_1 + B_3X_3 - L_2 & P_2 \\ V_3 = I_2X_2 - L_3 & P_3 \\ V_4 = I_3X_3 - L_4 & P_4 \end{cases} \quad (3)$$

Where, V_1 is the image point coordinate correction vector, V_2 is the POS observation correction vector, V_3 is the object point coordinate correction vector, and V_4 is the correction vector for systematic error observations such as POS system eccentricity angle and datum transformation parameters; X_1 is the exterior orientation element correction vector, X_2 is the object coordinate correction vector, and X_3 is the correction vector for compensation parameters of systematic errors such as collimation axis eccentricity angle and datum transformation parameters of POS system observations; L_i , A_i , P_i are the corresponding various observation values, coefficient matrices and weight matrices.

All parameters are solved simultaneously by least squares adjustment to achieve accurate calibration of the camera and POS system.

2.3 Positioning Method Without Ground Control Points Method

In order to achieve high-precision positioning of aerial images without GCPs, this manuscript proposes a “cloud control” photogrammetry method based on global public Google images and SRTM data. This method uses the characteristics of high absolute positioning accuracy and large-range spatial consistency of Google images and SRTM as auxiliary data sources for aerial image geolocation. The specific processing flow is as follows:

First, rough geometric correction of newly acquired aerial images is performed using initial exterior orientation angles (φ,ω,κ) derived from the POS system, mitigating distortions induced by attitude variations.Let the image point coordinates of the new image be (x,y), and the corresponding object point coordinates be (X,Y,Z), then the correction process can be expressed as formula (4):

$$\begin{bmatrix} x' \\ y' \end{bmatrix} = K \cdot R(\omega, \phi, \kappa) \cdot \begin{bmatrix} X - X_s \\ Y - Y_s \\ Z - Z_s \end{bmatrix} \quad (4)$$

Where, (x',y') is the corrected image point coordinate, K is the camera interior parameter matrix, R is the rotation matrix, and (X_S,Y_S,Z_S) is the photographic center coordinate.

Subsequently, a projective transformation between the newly acquired images and the reference Google images is established by image registration. Assuming an affine transformation model, the relationship is described as formula (5):

$$\begin{bmatrix} u \\ v \end{bmatrix} = \begin{bmatrix} a_{11} & a_{12} & t_x \\ a_{21} & a_{22} & t_y \end{bmatrix} \cdot \begin{bmatrix} x \\ y \\ 1 \end{bmatrix} \quad (5)$$

Where, (u,v) is the reference image coordinate, (x,y) is the coordinate of the image to be corrected, $A = [a_{11}, a_{12}; a_{21}, a_{22}]$ is the transformation matrix, and $T = [t_x,t_y]^T$ is the translation vector.

This above transformation enables resampling of the aerial image to align with the geometric datum and perspective of the base reference.

Thereafter, the SIFT feature matching algorithm is employed to identify homologous points between the corrected aerial images and Google images, constructing a free network of the new image. Through the matching results, the augmented points are transferred into the Google image space, and their object coordinates are determined by spatial forward intersection based on the high-precision exterior orientation parameters of the reference imagery (formula (6)):

$$X = \frac{(b_1 \cdot c_2 - b_2 \cdot c_1)}{(a_1 \cdot b_2 - a_2 \cdot b_1)},\ Y = \frac{(a_2 \cdot c_1 - a_1 \cdot c_2)}{(a_1 \cdot b_2 - a_2 \cdot b_1)} \quad (6)$$

Where, a_i,b_i,c_i are the coefficient matrix elements formed by linearizing the collinear condition equation.

The resulting three-dimensional coordinates of the augmented points serve as control data for subsequent bundle adjustment and geometric refinement, enabling high-accuracy geopositioning independent of field-surveyed GCPs.

3. Experiment

The experimental data were acquired using the AFC-900II mosaic aerial survey camera system. As illustrated in Figure 2, this large-format camera system integrates four panchromatic and four multispectral camera units, providing a total pixel count of approximately 900 million. Each optical channel covers an identical field of view and is associated with 6, 6, 4, and 4 non-overlapping CMOS sub-arrays respectively. Through a 5×4 arrangement of 20 sub-arrays on a virtual focal plane, the system achieves wide-field imaging capability with an enhanced base-to-height ratio.

Figure 2.AFC-900II aerial survey camera.

In September 2023, an aerial survey was conducted over the Hanzhong region of Hubei Province, China, utilizing the X-8C airborne platform. The dataset was acquired at a flight altitude of 1,200 meters (Figure 3 and Figure 4), yielding images with approximately 5 cm ground sample distance. During the mission, a network of 200 ground control points was established throughout the study area to support subsequent accuracy assessment, as depicted in Figure 3.

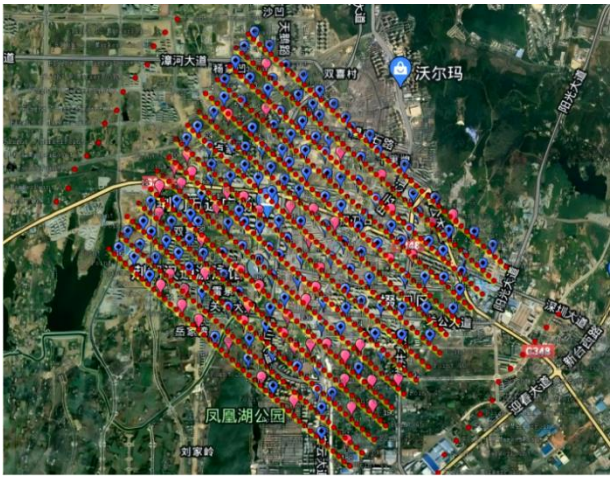

Figure 3.Schematic diagram of the experimental area and 200 ground check point locations.

Figure 4.Aerial photograph of part of the experimental area.

3.1 Cloud Control Point Extraction

Global public Google images and SRTM elevation data have high positioning accuracy and stability across broad geographical extents. As shown in Figure 5, these datasets were selected as the ground control data within the test area.

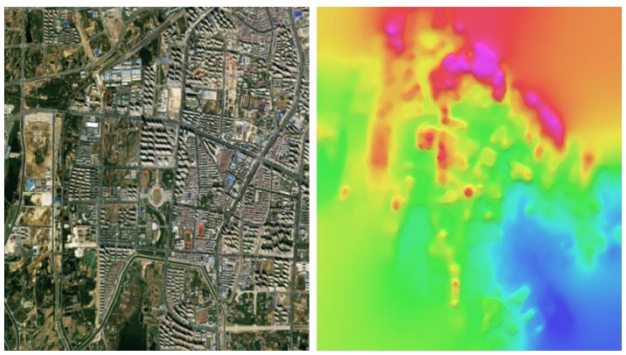

Figure 5. Google images and SRTM elevation data.

Using the orientation parameters derived by POS as initial exterior elements, we performed preliminary orthorectification to align the aerial imagery with the geometric characteristics of the Google Earth base. Subsequently, the feature matching method was employed to extract corresponding points between the datasets, enabling the generation of three-dimensional cloud control points by spatial intersection, as illustrated in Figure 6.

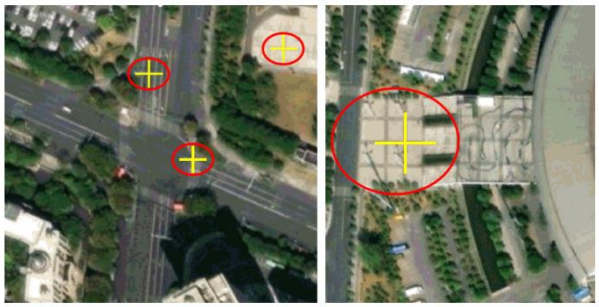

Figure 6.Information of some “cloud control points”.

3.2 Collimation Axis Error Calibration of Mosaic Aerial Survey Camera

Based on the control points acquired through the “cloud control” photogrammetric approach, the bundle block adjustment was performed to simultaneously estimate the exterior orientation parameters of each image and the collimation axis eccentricity angle of IMU. The obtained POS offset vector and IMU collimation axis eccentricity angle are shown in Table 1 and Table 2.

X error (cm)	Y error (cm)	Z error (cm)
7.45736	6.4993	0.685584

Table 1. POS offset vector.

IMU_φ（radian)	IMU_ω（radian)	IMU_κ（radian)
-0.002254	-0.0003841	-0.0078538

Table 2. IMU collimation axis eccentricity angles.

The calibrated POS offset vector is 7.45736 cm, 6.4993 cm, and 0.685584 cm in the X, Y, and Z directions respectively, and the IMU collimation axis eccentricity angles are -0.002254 rad, -0.0003841 rad, and -0.0078538 rad in the φ, ω, and κ directions respectively.

3.3 Virtual Image Generation and Accuracy Evaluation

The large-format panchromatic imagery was co-registered with multispectral data to generate a virtual mosaic image, as presented in Figure 7.

Figure 7. Final virtual mosaic image.

Subsequently, the POS data were refined using the calibrated offset vectors and IMU collimation axis eccentricity angle, followed by POS-assisted aerial triangulation to generate DEMs and orthophotos, illustrated in Figure 8, Figure 9 and Figure 10.

Figure 8. Overall orthophoto.

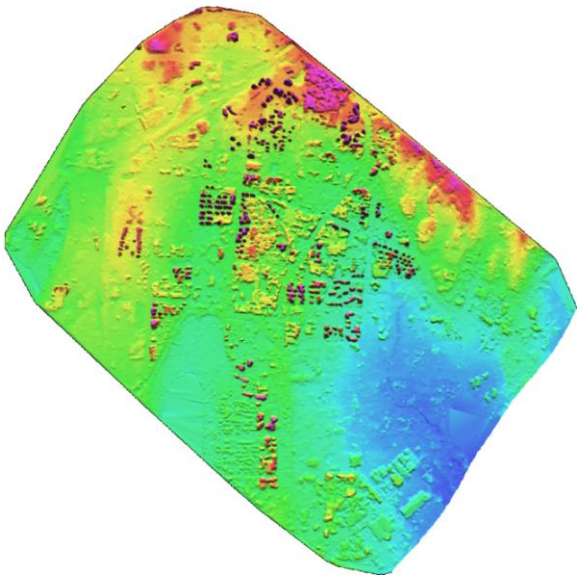

Figure 9. Overall DEM.

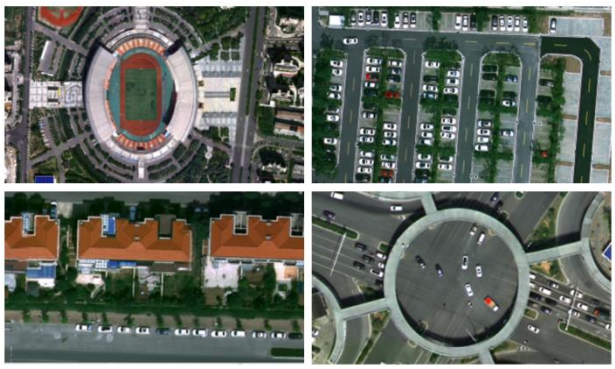

Figure 10. Partial orthophoto.

Finally, we used ground control points to evaluate the accuracy of DEMs and orthophotos. The planar accuracy is 0.29 meters in the x-direction and 0.40 meters in the y-direction, and the vertical accuracy is 0.78 meters, which is fully better than the assessment index (0.5 meters in planar accuracy and 0.8 meters in vertical accuracy), meeting the mapping requirements of 1:500 scale. The orthophoto generated after POS data correction and the actual coordinate distribution of control points are shown in Figure 11.

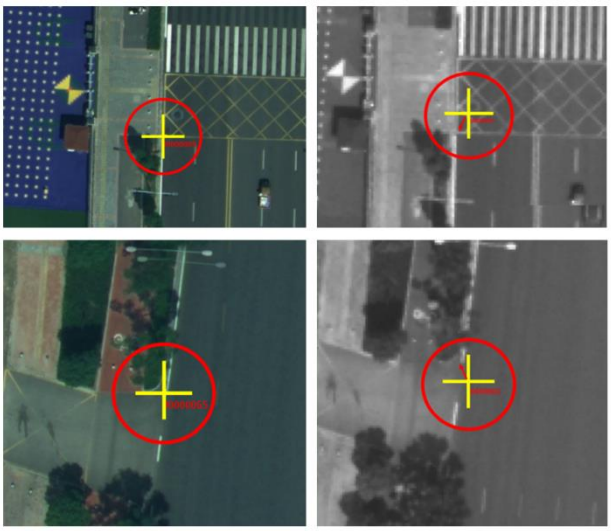

Figure 11. Orthophoto corrected by corrected POS data and coordinate position map of control points.

The errors of some control points are shown in Table 3.

Name	ΔX	ΔY	Horizontal	Vertical
A1	0.002	0.003	0.004	0.008
A2	0.003	0.003	0.004	0.008
A3	0.002	0.003	0.004	0.01
A4	0.003	0.003	0.004	0.01
A5	0.002	0.003	0.004	0.009
...	...	...	...	...
A51	0.003	0.002	0.003	0.006
A52	0.003	0.002	0.003	0.006
A53	0.003	0.002	0.003	0.006
A54	0.003	0.003	0.004	0.007
A55	0.003	0.002	0.003	0.006

Table 3. Check-point residuals (m).

4. Conclusion

This manuscript investigates collimation axis error calibration and GCP-free geopositioning for mosaic aerial survey cameras, with particular focus on “cloud control” error compensation methodology and positioning validation. The principal conclusions are as follows:

1) A high-precision collimation axis calibration method was developed for POS-camera integration in mosaic imaging systems. Addressing the inherent geometric discrepancies between multi-sensor configurations and POS references, the method establishes a collimation axis calibration model through multi-parameter joint optimization. By incorporating high-

precision external references obtained by "cloud control" technology, it achieves precise compensation of camera-POS installation deviations.

2) The feasibility of the GCP-free positioning framework was validated through practical aerial photogrammetric production experiments. Results demonstrate that the proposed collimation axis correction model coupled with rigorous geometric processing achieves planar accuracy of 0.29 m (x-direction) and 0.40 m (y-direction), with vertical accuracy of 0.78 m, meeting 1:500-scale surveying and mapping standards.

In conclusion, the proposed "cloud control" methodology for collimation axis calibration and GCP-free positioning effectively reduces field survey dependency, enhances operational efficiency, and provides a technically sound pathway for high-precision operational applications in aerial remote sensing surveying and mapping.

Acknowledgements

This study was supported by the Open Fund Project of Beijing Engineering Technology Research Center of Aviation Intelligent Remote Sensing Equipment, titled "Research on Ground-Control-Point-Free Positioning Technology for Mosaic Aerial Survey Systems".

References

Adu Gong, Xiaoying He, Tianjie Lei, and Jing Li. 2010. "Fast Image Processing Method of UAV without Control Data." *Journal of Geo-Information Science* 12 (2): 7.

Hao Cheng, Jie Cao, and Zhi Chen. 2016. "Stereo Positioning and Accuracy Analysis Based on the Double Image of No Control Point of UAV." *Electronic Design Engineering* 24 (11): 4.

Heng Lu, Yongshu Li, Jing He, and Zhiming Ren. 2011. "Capture and Processing of Low Altitude Remote Sensing Images by UAV." *Engineering of Surveying and Mapping* 20 (1): 4.

Huaiwu Ma, and Junqiang Wang. 2014. "Application of RTK Combined with UAV Photogrammetric in Surveying and Mapping of Plateau." *Journal of Geomatics* 39 (3): 4.

Jacobsen, Karsten. 2002. "Calibration Aspects in Direct Georeferencing of Frame Imagery." *International Archives of Photogrammetry Remote Sensing and Spatial Information Sciences* 34 (1): 82–88.

Jianhong Fu, and Shuangming Zhao. 2011. "Boresight Misalignment Calibration of Airborne Position and Orientation System Based on Photo Nadir Point." *Journal of Geodesy and Geoinformation Science* 40 (5): 6.

Liu, Jianchen, Rumeng Li, and Wei Guo. 2024. "POS Assisted Aerial Triangulation Method for Single Flight Strip without Ground Control Points." *IEEE Journal of Selected Topics in Applied Earth Observations and Remote Sensing* 17: 6328–37.

Mikš, Antonín, and Jiří Novák. 2018. "Analysis of the Optical Center Position of an Optical System of a Camera Lens." *Applied Optics* 57 (16): 4409–14.

Qiuhui Xu. 2013. "A Method of Geometric Correction and Mosaic of Unmanned Aerial Vehicle Remote Sensing Image without Ground Control Points." Nanjing University.

Salas López, Rolando, Renzo E. Terrones Murga, Jhonsy O. Silva-López, et al. 2022. "Accuracy Assessment of Direct Georeferencing for Photogrammetric Applications Based on UAS-GNSS for High Andean Urban Environments." *Drones* 6 (12): 388.

Shulei Ding. 2024. "Research on DEM-Assisted Satellite Image Positioning withoutGround Control Point." Lanzhou Jiaotong University.

Xin Jia, Shuwen Yang, Zhihua Zhang, and Ruliu Yan. 2019. "A Method to Improve Positioning Accuracy of UAV Image Based on POS Data." *Remote Sensing Information* 34 (4): 5.

Xiuxiao Yuan, Fen Yang, Qing Zhao, and Yang Ming. 2006. "Boresight Misalignment Calibration of Integrated DGPS/IMU System." *Geomatics and Information Science of Wuhan University* 31 (12): 1039–43.

Yushan Sun, Li Zhang, Biao Xu, and Yong Zhang. 2018. "Method and GCP-Independent Block Adjustment for ZY-3 Satellite Images." *National Remote Sensing Bulletin*, no. 2.

Zhu, Xiaokun, Chen Liang, Huimin Tian, Mingce Xu, and Yutao Guo. 2025. "Intelligent Processing Technology for Time-Series Archived Historical Aerial Photos Based on Cloud Control Photogrammetry." *Sensors and Materials* 37 (Compendex): 1449–58. https://doi.org/10.18494/SAM5302.

Zuxun ZHANG, Xinbo ZHAO, and Yansong DUAN. 2025. "A block-wise polynomial distortion model for airborne composite large-format camera." *Acta Geodaetica et Cartographica Sinica* 54 (1): 52–63.